Available online at www.sciencedirect.com

SciVerse ScienceDirect

Ceramics International 39 (2013) 519–528

CERAMICS INTERNATIONAL

www.elsevier.com/locate/ceramint

Hydrolysis of Ca-deficient hydroxyapatite precursors in the presence of alanine-functionalized polyphosphazene nanofibers

Y.E. Greish[a,*,1], J.D. Bender[b], A. Singh[c], L.S. Nair[d], P.W. Brown[e], H.R. Allcock[f], C.T. Laurencin[d]

[a]*Department of Chemistry, Faculty of Science, United Arab Emirates University, Al Ain, P.O.Box17551,UAE*
[b]*Air products and Chemicals, Inc., Allentown, PA 18103, USA*
[c]*Dow Global Technologies LLC, Midland, MI 48674, USA*
[d]*Department of Chemical, Materials and Biomolecular Engineering, Institute of Material Science, University of Connecticut, Farmington, CT06030, USA*
[e]*Materials Research Laboratory, The Pennsylvania State University, University Park, PA 16802, USA*
[f]*Department of Chemistry, The Pennsylvania State University, University Park, PA 16802, USA*

Received 7 April 2012; received in revised form 10 June 2012; accepted 19 June 2012
Available online 27 June 2012

Abstract

Hard tissues are made of nanoapatite crystallites grown on a nanofibrous collagen matrix. The mechanical interlocking and the chemical bonding between both phases provide the unique properties of hard tissues. A biodegradable alanine-substituted polyphosphazene nanofibrous scaffold was prepared by an electrospinning technique. Scaffolds were loaded with precursors that form Ca-deficient hydroxyapatite upon hydrolysis in aqueous media. Composite scaffolds containing 30, 60, and 90 wt% were subjected to hydrolysis in a phosphate buffer solution for up to 10 days, and was followed by pH measurements, x-ray diffraction and scanning electron microscopy. Results showed a delayed conversion of the precursors into Ca-deficient apatite, which was proven to be attributed to the encapsulation of the precursors within the polymer nanofibrous scaffold and the slow introduction of water of hydrolysis to the precursors. This was accompanied by an increasing swelling of the nanofibers. An overall buffering effect took place within the system as a result of the degradation of the polymeric nanofibers, maintaining pH of the media within physiologic pH values.

Keywords: Calcium-deficient hydroxyapatite; Hydrolysis; Nanofibers; Polyphosphazene

1. Introduction

The unique properties of hard tissues are attributed to the composition and construction of its components [1]. Two main components are responsible for these properties: collagen and hydroxyapatite. The later, ($Ca_{10}(PO_4)_6(OH)_2$; HAp), is in the form of nanocrystals that are interlocked with the nanofibers of the former [1]. In order to simulate the structure and properties of natural hard tissues, researchers have investigated the fabrication of composites based on synthetic HAp and biocompatible polymers. Synthetic HAp could be obtained by different routes, among which low temperature cement-type reactions have been widely studied [2–6]. In the work of Brown and Chow in 1987, a low temperature bone-like apatite was produced from a simple hydrolysis process of a mixture of acidic and basic calcium phosphates. Precursors used in these studies included tetracalcium phosphate ($Ca_4(PO_4)_2O$; TetCP) as a basic precursor with a Ca/P ratio of 2.0, and acidic precursors which have lower Ca/P molar ratios such as anhydrous dicalcium phosphates ($CaHPO_4$; DCPA and $CaHPO_4 \cdot 2H_2O$; DCPD). Reaction between TetCP and DCPA or DCPD took place in aqueous media at physiologic temperatures forming a set product of apatitic nature with a Ca/P ratio that depends on the original Ca/P ratio of the starting precursors. Eqs. (1) and (2) illustrate the dependence of the formed apatite on the stoichiometry of the starting reactants.

$$2CaHPO_4(2H_2O) + 2Ca_4(PO_4)_2O \rightarrow Ca_{10}(PO_4)_6(OH)_2 \quad (1)$$

*Corresponding author. Tel.: +971 50 2338203.
E-mail address: y.afifi@uaeu.ac.ae (Y.E. Greish).
[1]Permanent address: Department of Ceramics, National Research Centre, Cairo, Egypt.

0272-8842/$36.00
http://dx.doi.org/10.1016/j.ceramint.2012.06.057

$$3CaHPO_4(2H_2O) + 1.5Ca_4(PO4)_2O \rightarrow Ca_9(HPO_4)(PO_4)5OH \quad (2)$$

Apatites with Ca/P lower than 1.67 are non-stoichiometric and are called Ca-deficient apatites, which are also known to be more bioactive compared to stoichiometric apatite with a Ca/P ratio of 1.67 [4].

When used for in vivo applications, cement pastes comprising mixtures of Ca-deficient or stoichiometric apatite precursors can be injected or sculpted during surgery into the bone defect site where it hardens to form bone-like apatite [7–9]. These cements provide exceptional contact between the bone and the graft and hence they are osteointegrative [10]. In addition, due to their low temperature fabrication, these cements have been also investigated for drug delivery applications [11].

Calcium-deficient HAp with a Ca/P molar ratio of 1.5 has been prepared using low temperature cement-type reactions involving different precursors such as TetCP/DCPA [12], TetCP/DCPD [7], as shown in Eq. (2), and neat α-$Ca_3(PO_2)_2$, as shown in Eq. (3) [13].

$$3\alpha\text{-}Ca_3(PO_4)_2 \xrightarrow{H_2O} Ca_9(HPO_4)(PO_4)_5OH \quad (3)$$

This type of apatite is characterized by enhanced bioactivity and its ability to be remodeled through dissolution–precipitation mechanism of the set cement after implantation [14]. Recently, we have developed a novel type of Ca-def apatite with a Ca/P ratio of 1.6, known thereafter as CDSH [10]. This molar ratio was achieved by adjusting the proportions of TetCP and DCPA in the original powder mixture prior to their hydration in aqueous media. CDSH was previously evaluated for its osteocompatibility using MC3T3-E1 cells and was proven comparable to tissue culture polystyrene [10]. Moreover, CDSHA expressed the characteristic genes for OsteoPontin, OsteoCalcin, Alkaline phosphatase, and type I collagen which are usually expressed by osteoblast cells during differentiation, maturation and mineralization [10]. Combining the characteristics of CDSH with biodegradable polymers is highly thought to produce composites that can be used for bone regeneration applications.

Biodegradable polymers such as poly(hydroxyl esters) have been widely investigated for tissue regeneration applications; either in their neat form or as composites with HAp [15–18]. However, toxic effects attributed to the low pH of their acidic degradation products have limited their applications [19,20]. In contrast, biodegradable polyphosphazenes maintain the physiologic pH conditions and do not cause cytotoxicity [21]. Polyphosphazenes differ from traditional carbon-based polymers in that their backbones are made of phosphorous and nitrogen atoms with two side groups attached to each phosphorous atom [21]. Biodegradable polyphosphazenes with phosphorous atoms attached to specific side groups such as imidazolyl and amino acid esters undergo hydrolysis to yield non-toxic degradation products [21]. The degradation products of polyphosphazenes consist of ammonia, phosphates, and the corresponding side groups [22]. Ammonia and phosphates constitute a buffer system which can stabilize the pH of the system effectively in comparison with poly-(hydroxyesters) [19]. Biodegradable polyphosphazenes bearing amino acid esters as side groups have shown excellent biocompatibility and hence are promising candidates for different biomedical applications such as tissue engineering and drug delivery [21,23–25]. A potential candidate in this class of biodegradable polyphosphazenes is poly[bis(ethyl alanato) polyphosphazene] (PN-EA) which has been used for the regeneration of severed sciatic nerves in Wistar rats, and were slowly absorbed without any sign of general or local toxicity with regeneration of nerves similar to autologous grafts [24,26]. Moreover, PN-EA implanted subcutaneously was shown to elicit minimal inflammatory responses after 12 weeks of implantation [27].

Cement composites containing HAp with PN-EA were previously evaluated at physiologic conditions [10,28–29]. Pre-prepared stoichiometric nano HAp was blended with PN-EA in its proper solvent and electrospun into composite nanofibers at a maximum HAp loading of 60% by weight [28]. Hydrolysis of Ca-deficient HAp precursors with Ca/P ratios of 1.5; CDH and 1.6; CDSH in the presence of PN-EA powder was also investigated in aqueous media [10,29]. In these studies, hydrolysis of the ethyl ester of PN-EA took place forming ionized carboxylate groups ($-COO^-$). As a result, cross links were formed between the Ca^{2+} ions released during the hydrolysis of CDH (or CDSH) and the PN-EA formed COO^- groups. It was found, however, that the high pH regime obtained during the hydrolysis of CDSH was not affected by the buffering capacity caused by the degradation of PN-EA. In the current study, the in situ hydrolysis of CDSH precursors while encapsulated within PN-EA nanofibrous scaffolds is investigated. With the advantages of high surface area and interconnected porosity in nanofibrous scaffolds, a combination of bone-like CDSH and biodegradable PN-EA nanofibers is highly thought to serve as scaffold for bone tissue regeneration.

2. Materials and methods

Precursors used for making CDSH included TetCP, and DCPA. In order to have better reaction kinetics, an intimate powder mixture of these salts was obtained by a mechanochemical reaction of TetCP with monocalcium phosphate monohydrate ($Ca(H_2PO_4)_2 \cdot H_2O$; MCPM) (FMC Corp., NY) at a Ca/P ratio of 1.6. This reaction was previously established by Martin and Brown [12], and is shown in the following equation:

$$Ca(H_2PO_4)_2H_2O + 7Ca_4(PO_4)_2O \rightarrow 6CaHPO_4 + 6Ca_4(PO_4)_2O + 3H_2O \quad (4)$$

TetCP was synthesized as previously described [30]. After confirming phase purity by x-ray diffraction, TetCP powder was ground to an average particle size of 2.5 μm,

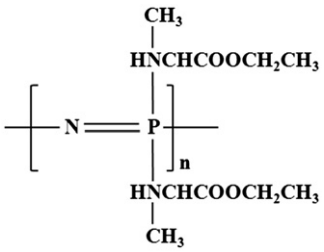

Scheme 1. Structure of PN-EA

as determined by scanning electron microscopy (SEM). PN-EA was synthesized using a two-step macromolecular substitution process as described in previous articles [28]. In brief, polydichlorophosphazene, as a starting ingredient, was first prepared by the thermal ring opening polymerization of hexachlorocyclotriphosphazene by heating at 250 °C under vacuum. In the second step, complete replacement of the chlorine atoms in poly(dichlorophosphazene) with alanine ethyl ester groups was carried out. The produced PN-EA polymer (Scheme 1) was isolated by precipitation in hexane, then purified by re-precipitation from hexane (3×) to obtain a tough white polymer. Molecular weight measurements showed an average weight molecular weight value (M_w) of 1.7×10^5.

Solutions containing 9% w/v of PN-EA in THF were prepared by a vigorous dissolution of fine PN-EA powder in THF. To these solutions, CDSH precursors were added at weight percentages of 30, 60, and 90 wt%. The produced suspensions were vigorously stirred until homogenous slurries were obtained. Both pure PN-EA and CDSH-containing PN-EA solutions were electrospun at the pre-optimized conditions of 15 kV operating voltage, a flow rate of 2 mL/h and a spinning distance of 30 cm [31]. The obtained nanofibrous mats were collected then examined for their phase composition and microstructure using x-ray diffraction (XRD) and scanning electron microscopy (SEM), respectively. X-ray diffraction analysis was performed using a Scintag diffractometer (Scintag Inc., Sunnyvale, CA), with a step size of 0.02°, and a scan rate of 2° per minute, over a 2 theta range of 20–40°. Phases present in the XRD patterns were compared to powder diffraction cards (PDF) 25-1137, 9-80 and 9-432 which correspond to TetCP, DCPA and HAp phases, respectively. A semi-quantitative formula, shown below, was used to calculate the % composition of HAp, TetCP, and DCPA in the as-spun nanofibrous composite mats and throughout the hydrolysis process [3]:

$$\%I_i = \left[\frac{I_i}{I_1+I_2+I_3}\right]$$

where I_i is the phase of concern, i=1,2,3; I_1 corresponds to the intensity of the HAp 002 peak at 2θ=25.9°; I_2 corresponds to the intensity of the HAp 200 peak at 2θ=25.4°; I_3 corresponds to the intensity of the HAp 112 peak at 2θ=30.5°.

These peaks were chosen based on the fact that they do not overlap in the XRD patterns of their mixtures.

SEM analysis was carried out on gold coated scaffolds using a conventional dual-stage scanning electron microscope (SEM) (Philips 420T) equipped with an energy-dispersive x-ray (EDX) analyzer at an operating voltage of 20 KeV. Mapping of the elements in selected areas of CDSH-containing scaffolds was also examined using EDX. In addition, surface area, porosity and pore size distribution of the nanofibrous scaffolds were examined using nitrogen gas adsorption at 77 K employing a Quantochrome NOVA 1000 volumetric gas sorption instrument; Autosorb, USA.

Hydrolysis reactions were carried out in phosphate buffer solutions (PBS). In brief, square-shape samples (2.5 cm × 2.5 cm × 0.2 cm) of neat PN-EA and CDSH/PN-EA scaffolds were immersed in vials containing 50 ml of PBS, and incubated at a physiologic temperature of 37.4 °C under N_2 atmosphere for up to 10 days. Variation in the pH of these solutions with time was followed using an Orion 920 pH meter. Scaffolds were also examined for their phase composition and microstructure after 1, 7 and 10 days of immersion in PBS. Hydrolysis of pure polymer-free CDSH precursors' mixture was also carried out at the same conditions for comparison.

3. Results and discussion

Hydrolysis of stoichiometric and Ca-deficient HAp precursors, SHAp (Ca/P 1.67) and CDH (Ca/P 1.5) respectively, has been previously studied in details. Despite the equality of the molar ratio of TetCP and DCPA in the SHAp precursors mixture, the preferential solubility of TetCP produces highly basic media [3]. In contrast, the hydrolysis of CDH precursors tends to provide slightly acidic media due to the domination of the mixture with the acidic salt, DCPA [12]. Hydrolysis of the polymer-free CDSH precursors takes place in an intermediate fashion until completion in 24 h. Fig. 1A shows the variation in pH of the solution as a result of these reactions. Hydrolysis reactions take place through dissolution of the reactants, TetCP and DCPA, enriching the medium with Ca^{2+} and PO_4^{3-} ions. These ions re-precipitate in the form of calcium-deficient HAp, CDSH. Fig. 1A shows a sudden increase in the pH of the medium within the first hour of hydration reaching a pH of 8.8; shown as stage I. This is attributed to the dissolution of the basic precursor, TetCP [3]. This fast increase in pH was followed by another stage of pH increase at a slower rate over the following 6 h, achieving a maximum pH of 9.3 after 7 h; stage II in Fig. 1A. This was further followed by a third stage of pH increase with a relatively faster rate, stage III, achieving a maximum pH of 10.2 after 12.3 h. The overall increase in pH during the first three stages is attributed to continued dissolution of TetCP, and indicates that this reaction dominated the overall process during the first 12 h. It should be mentioned that the variation in the rate of

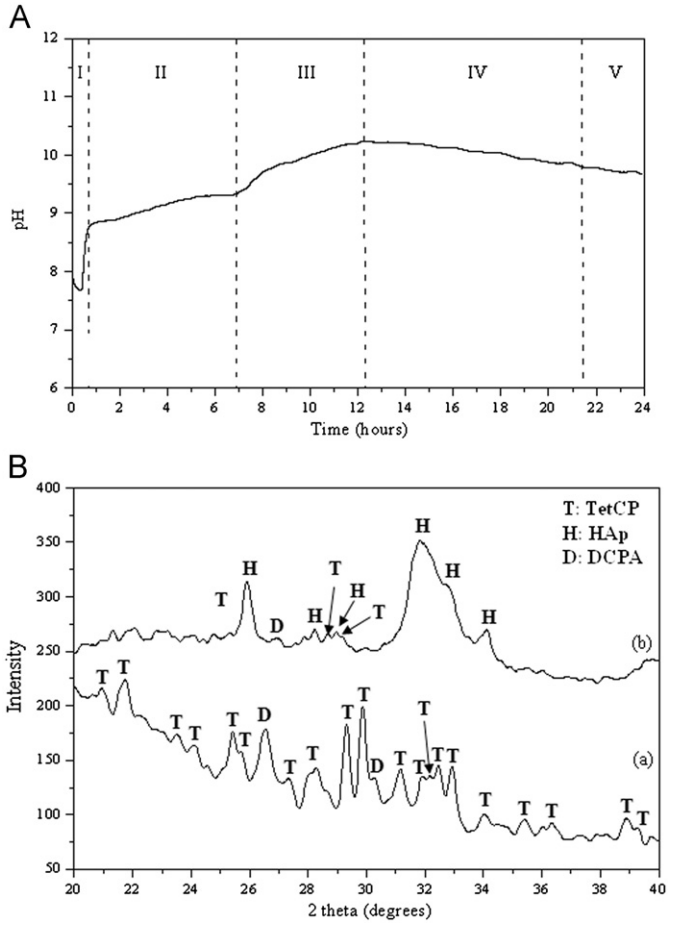

Fig. 1. (A) Variation of pH with time during the hydrolysis of CDSH precursors in aqueous media. (B) X-ray diffraction patterns of starting CDSH precursors (a) and final Ca-deficient HAp product (b).

pH increase during these stages is attributed to the participation of the acidic precursor, DCPA, in the dissolution reactions [3]. Compared to the dissolution of TetCP and DCPA during the process of formation of stoichiometric HAp [3], the medium with the highest pH achieved in the current system is less alkaline, which is attributed to the presence of TetCP in a lower proportion. A slower decrease in the pH of the medium was observed during the following 12 h achieving a value of 9.7 after 24 h of hydrolysis. This decrease in pH is attributed to the dissolution of the acidic precursor, DCPA, as a dominant reaction. Fig. 1B shows XRD patterns of starting powder mixture as compared with the formed CDSH. The XRD pattern of the starting powder mixture indicates the presence of TetCP and DCPA reactants, while that of the formed product is dominated by HAp with traces of unreacted TetCP and DCPA, as compared with their standard JCPDS cards. Taken together, results of Fig. 1 indicate that hydrolysis of Ca-deficient precursors in aqueous media is not entirely complete and that the pH of the medium at the end of 24 h is highly alkaline.

Fig. 2 shows the morphology of pure PN-EA scaffolds and those containing 30, 60 and 90 wt% of CDSH precursors before hydrolysis. It should be mentioned that electrospinning of the composite mixtures were carried out at the pre-optimized conditions. Therefore, all scaffolds were bead-free with a uniform fiber size distribution on average. Fibers with a uniform cylindrical morphology and a diameter ranging between 150 and 1000 nm were obtained at these conditions. Morphology of the electrospun scaffolds resembles that of the extracellular matrix (ECM), which strongly nominated these assemblies to be used for bone tissue regeneration. This is more supported by the biodegradable nature of PN-EA and the presence of apatitic precursors within the scaffolds. CDSH precursors are well distributed within the framework of the nanofibrous scaffolds. A closer look at the micrographs in Fig. 2b–d indicates that precursors were either mechanically integrated with the nanofibers or encapsulated within the nanofibers. Distribution of CDSH precursors within the nanofibrous scaffolds was further investigated by elemental mapping to confirm the homogeneity of distribution of the CDSH precursors within the nanofibrous assemblage shown in Fig. 3a. Distribution of Ca and P in Fig. 3b and c, respectively, indicates their homogeneity. The higher abundance of phosphorous in Fig. 3c is attributed to the presence of phosphorous in the structure of both CDSH precursors and PN-EA nanofibers. Fig. 3d shows EDX analysis of a solid CDSH precursors' assembly, while that in Fig. 3e for a selected PN-EA nanofiber. The Ca/P molar ratio of the starting CDSH precursors is previously adjusted at 1.6, while that calculated from Fig. 3d gives a lower Ca/P value of 1.16. This is related to the presence of these precursors within the nanofibers that normally contain phosphorous in their backbone. The EDX graph in Fig. 3e also shows the presence of a low proportion of calcium which is attributed to the CDSH near and within the investigated nanofibers. Composition of these precursors was also analyzed by XRD, Fig. 2e, for nanofibrous scaffolds containing different proportions of CDSH precursors. These diffraction patterns indicate the continued presence of starting reactants, TetCP and DCPA, and the absence of any traces of CDSH. These results were expected since CDSH-polymer suspensions were initially prepared in non-aqueous media where hydrolysis reactions did not take place.

The presence of CDSH precursors within the assemblage of PN-EA nanofibers resulted in a relative decrease in the surface area of the scaffolds. Neat PN-EA nanofibrous scaffold showed a surface area of $55 \pm 0.07\ m^2/g$, while scaffolds containing 30, 60, and 90 wt% CDSH precursors showed surface area values of 52 ± 0.08, 41 ± 0.05 and $37 \pm 0.05\ m^2/g$, respectively. Comparing these results to the SEM micrographs in Fig. 2 which show the same average size of PN-EA nanofibers indicates that the decrease in surface area is attributed to the presence of increasing proportions of CDSH precursor grains with an average size of 3 μm in the composite scaffolds. One of the advantages of nanofibrous scaffolds is the presence of interconnected pores, as indicated from the micrographs in

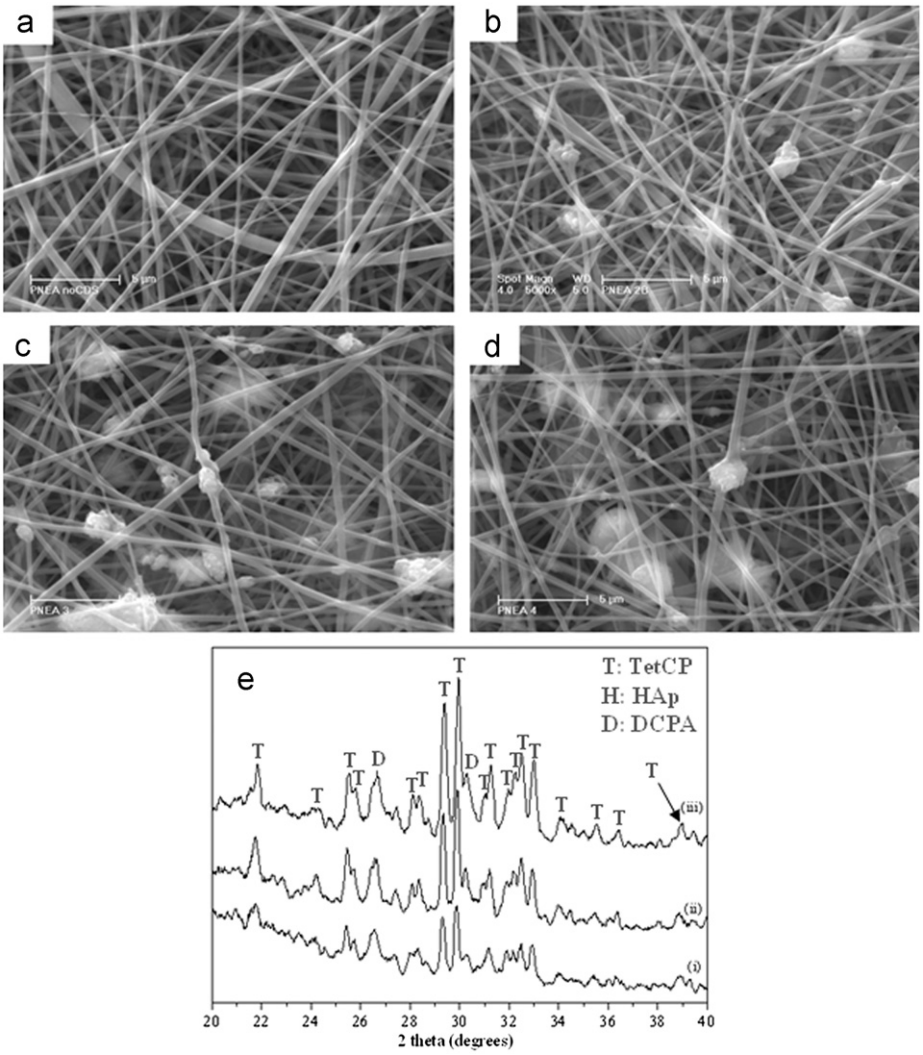

Fig. 2. Scanning electron micrographs of as spun (a) pure PN-EA nanofibers and nanofibrous scaffolds containing (b) 30, (c) 60, and (d) 90 wt% CDSH precursors, (e) X-ray diffraction pattern of nanofibrous scaffolds containing (i) 30, (ii) 60, and (iii) 90 wt% CDSH precursors.

Fig. 2 of as-spun scaffolds. Pore size distributions of the CDSH-containing scaffolds are shown in Fig. 4b–d. Pores within the range of 0.5–100 μm are shown within the formed scaffolds, with most of the pores within a range of 80 ± 10 μm. This wide range of porosity is recommended for tissue engineering applications. Distribution of these pores was not affected by the increase in the proportion of CDSH precursors in the scaffolds, which could indicate that most of the CDSH grains are located within the nanofibers, keeping the same proportion of open pores in all scaffolds.

In situ hydrolysis of CDSH precursors within the nanofibers was carried out in a phosphate buffer solution. Fig. 5 shows micrographs of neat and CDSH-containing PN-EA nanofibrous scaffolds after 7 days of hydrolysis. A pronounced increase in the diameter of the nanofibers was observed in all scaffolds, which is attributed to swelling of the nanofibers. Moreover, an increase in the roughness of nanofibers surfaces was also observed. Swelling of PN-EA was previously observed in alanine co-substituted polyphosphazenes and PN-EA composites with pre-made nano HAp and Ca-deficient HAp with Ca/P molar ratios of 1.5 and 1.6 [28,29]. Swelling of PN-EA nanofibers was more pronounced in the current study compared with pure PN-EA films and its composites with HAp, which is related to the higher surface area of the PN-EA nanofibers in the current study. In addition and because of the relatively low initial molecular weight of PN-EA, this allowed a greater degree of swelling and thus more water uptake. Swelling and surface roughness of the nanofibers were even more pronounced when the scaffolds were further soaked in the phosphate buffer for up to 10 days. Fig. 6a and b shows micrographs of composite scaffolds containing 30 and 90 wt% CDSH. As a result of swelling of the nanofibers, porosities of the scaffolds were highly affected. Fig. 7 shows the decrease in porosity of a composite scaffold containing 30 wt% CDSH precursors as a result of immersion in PBS buffer for up to 10 days. Porosity of these scaffolds decreased from $85 \pm 3.1\%$ to $30 \pm 2.3\%$ for scaffolds soaked in PBS buffer for 1 and

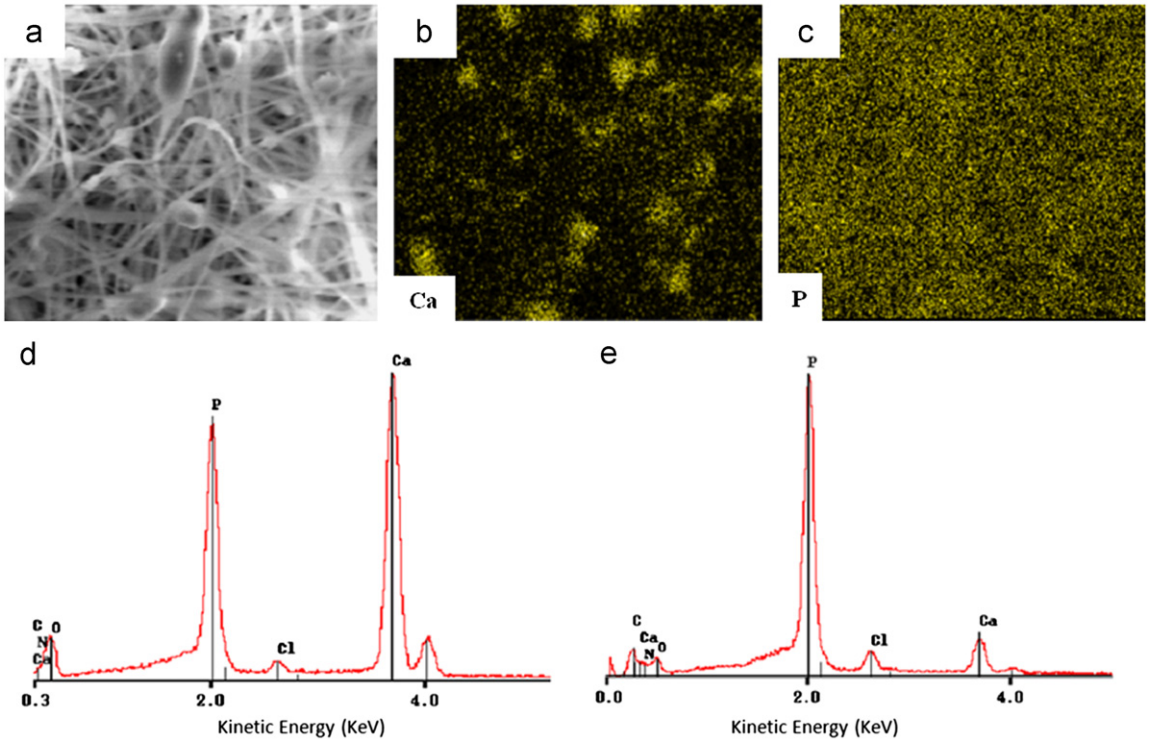

Fig. 3. (a) Scanning electron micrograph of a PN-EA nanofibrous scaffold containing 90 wt% CDSH precursors. Elemental mapping of (b) calcium, and (c) phosphorous atoms. EDX spectrum of (d) CDSH precursors encapsulated in the nanofibers, and (e) PN-EA nanofibers.

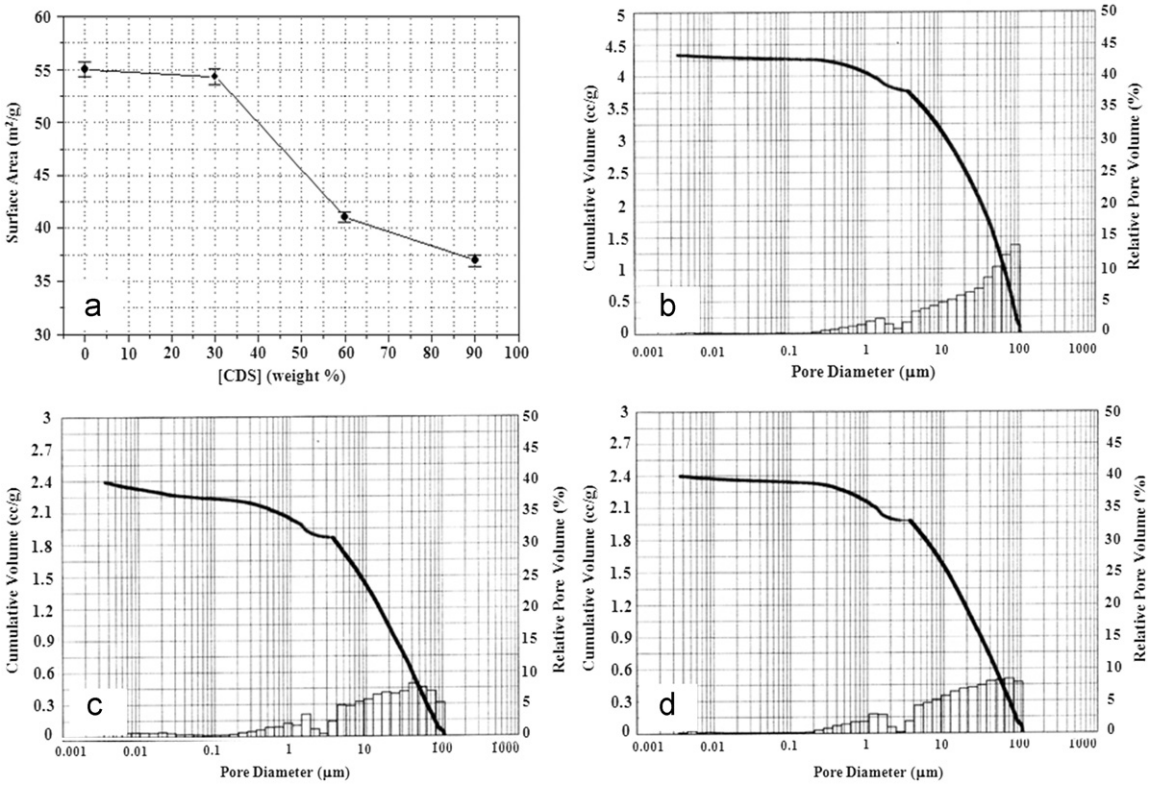

Fig. 4. (a) Variation of surface area of neat and CDSH-containing PN-EA nanofibers, and pore volume distribution of as spun nanofibrous scaffolds containing (b) 30, (c) 60, and (d) 90 wt% CDSH precursors.

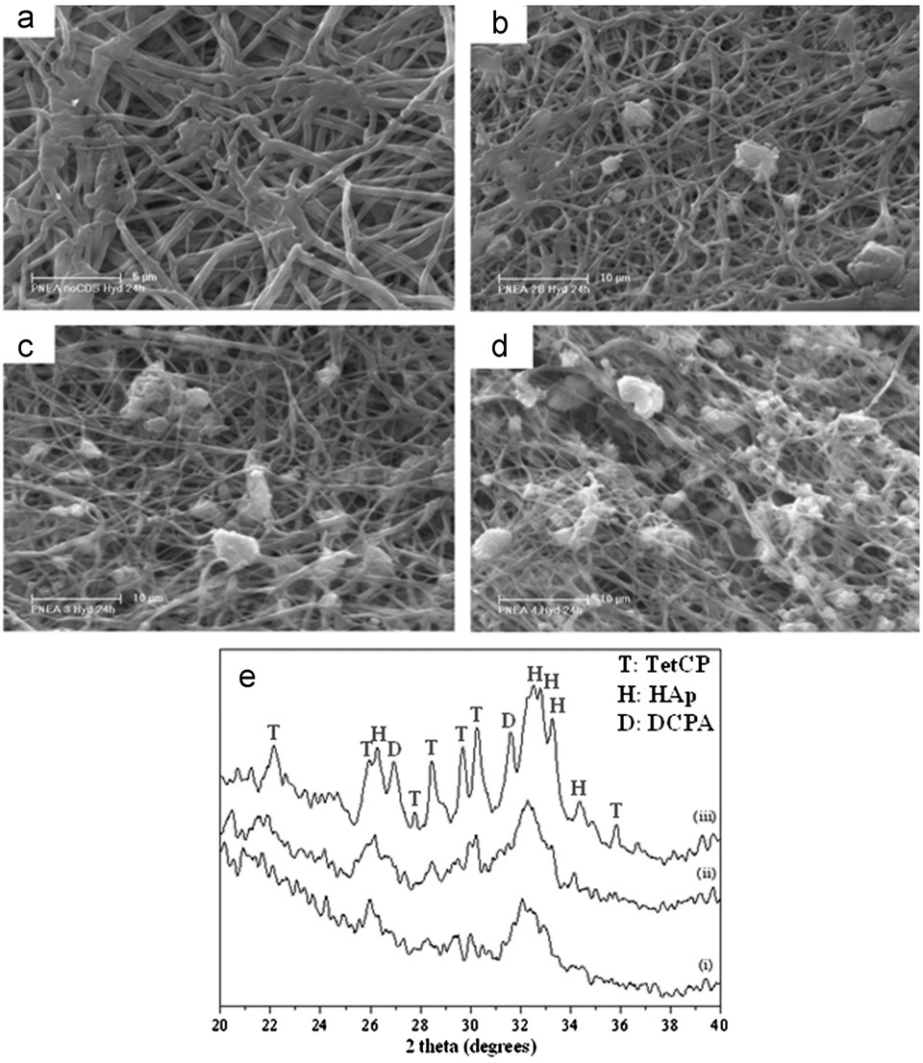

Fig. 5. Scanning electron micrographs of (a) pure PN-EA nanofibers and nanofibrous scaffolds containing (b) 30, (c) 60, and (d) 90 wt% CDSH precursors, (e) X-ray diffraction pattern of nanofibrous scaffolds containing (i) 30, (ii) 60, and (iii) 90 wt% CDSH precursors after hydrolysis for 7 days in aqueous media.

10 days, respectively. This is attributed to the observed increase in the diameter of the nanofibers as a result of swelling, and the subsequent decrease in the spacings, porosity, between these fibers.

Fig. 5e illustrates the variation in composition of the CDSH precursors as a result of their hydrolysis while encapsulated within the PN-EA nanofibrous scaffolds. The XRD patterns shown in Fig. 5e indicate a delayed conversion of the precursors into CDSH in composite scaffolds containing 90 wt% precursors. On the other hand, composite scaffolds containing 30 and 60 wt% CDSH precursors showed the formation of CDSH as a major phase with traces of TetCP and DCPA reactants. Despite the near complete conversion of precursors into CDSH, as shown in Fig. 1b, the delayed formation of CDSH within the PN-EA nanofibers is attributed to the encapsulation of the precursors within the nanofibers. This has limited the interaction between the precursors and the aqueous media required for the hydrolysis reaction to take place. Continued soaking in the buffer solution for 10 days resulted in an increased conversion of precursors into apatitic CDSH in all composite scaffolds, as shown in the XRD patterns in Fig. 6c. A summary of the phase evolution over time in all samples is shown in Fig. 8, which clearly illustrates the disappearance of TetCP and DCPA phases with the concurrent formation of apatitic CDSH. It should be mentioned that the continued water uptake and swelling of the fibers resulted in the introduction of water for hydrolysis of the precursors while encapsulated within the PN-EA nanofibers.

In contrast to the hydrolysis of pure CDSH precursors in PBS buffer, sustained hydrolysis of CDSH precursors over a longer course of time has resulted in a different manner of variation in pH of the aqueous media in which composite scaffolds were soaked, Fig. 9. An increase in the pH of all media took place within the first hour of hydrolysis achieving maximum pH values of 7.1, 7.2 and 7.5. in scaffolds containing 30, 60, and 90 wt% of CDS

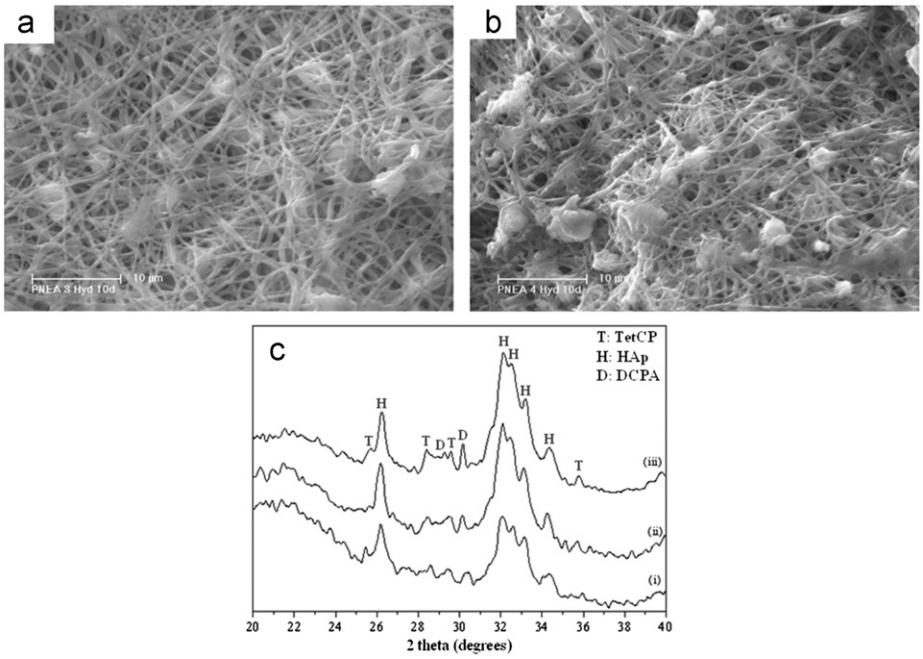

Fig. 6. Scanning electron micrographs of nanofibrous scaffolds containing (a) 30, and (b) 90 wt% CDSH precursors. (c) X-ray diffraction pattern of nanofibrous scaffolds containing (i) 30, (ii) 60, and (iii) 90 wt% CDSH precursors after hydrolysis for 10 days in aqueous media.

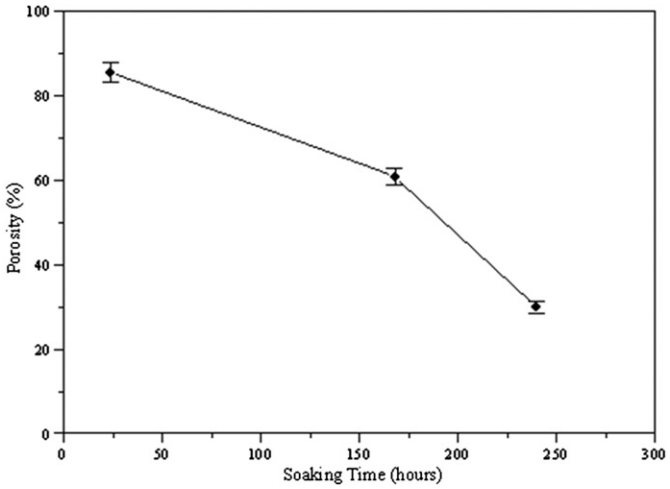

Fig. 7. Variation of percent porosity of PN-EA nanofibrous scaffolds containing 30 wt% CDSH precursors as a result of hydrolysis in aqueous media for up to 10 days.

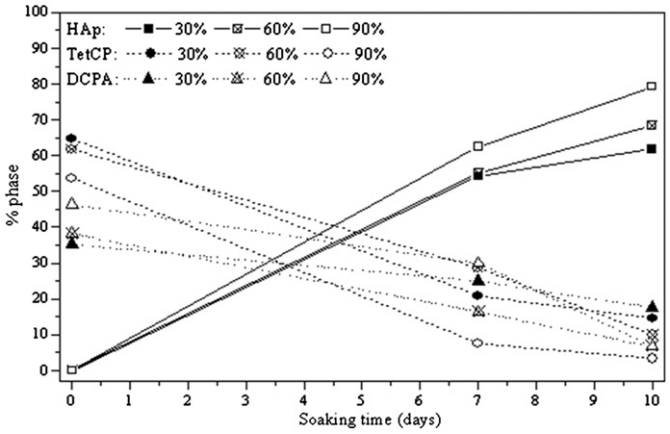

Fig. 8. Variation of percent phase composition during the hydrolysis of CDSH precursors for up to 10 days.

precursors, respectively. This is attributed to the dissolution of the basic precursors, TetCP. However, compared to a pH value of 8.8 reached during the hydrolysis of pure CDSH precursors in PBS buffer, Fig. 1A, the lower pH values achieved in solutions containing composite scaffolds indicate the relatively lower rate of dissolution of TetCP. During the following 12 h of hydrolysis, pH values of all media were maintained at 7.2, 7.25, and 7.6, which are also the maximum values achieved throughout the entire duration of hydrolysis of these composite scaffolds. This could be explained by the slow dissolution of TetCP, the basic precursor, in the soaking media and the buffering effect caused by the onset of degradation of PN-EA nanofibers. In a previous study, degradation of PN-EA films in PBS solution was also monitored by recording mass loss over a period of 7 weeks. PN-EA films showed a substantial weight loss of 40% by the end of the first week of immersion [30]. Two mechanisms have been established for the degradation of PN-EA. In both mechanisms, degradation takes place through a random chain scission of the P–N backbone. Detailed degradation takes place through the hydrolysis of the ester units of the side groups to form the corresponding polymer-bound alanine with a

deprotected carboxylic acid unit. The phosphorus atoms in the backbone are then susceptible to attack by the carboxylic acid units. In the second mechanism, it has been suggested that water displaces the amino acid esters from the phosphorus atoms to form a hydroxyphosphazene species, which then undergoes chain cleavage to phosphates and ammonia. In both proposed mechanisms, it is the formation of hydroxyphosphazene species that is responsible for the hydrolytic instability of the polymer. The hydrolysis products in both mechanisms were identified as phosphates, ammonia, amino acid, and the alcohol derived from the ester group on the amino acid unit [32]. These groups maintain the pH of the PBS buffer at its original physiologic value. In the present study, this phenomenon was more pronounced by virtue of the high surface area of PN-EA nanofibers. Despite the swelling and degradation of the nanofibers, their composite scaffolds remained intact while hydrolysis of CDSH precursors continued to take place leading to apatitic Ca-deficient product. Fig. 10 compares micrographs of encapsulated CDSH precursors before hydrolysis, Fig. 10a, with the hydrolysis apatitic CDSH product, Fig. 10b, in a composite scaffold containing 90 wt% CDSH precursors after 10 days of hydrolysis in PBS buffer. Despite the encapsulation of the precursors within the nanofibers, elongated apatitic CDSH crystals emerged out of the fibers with a composition that was previously shown in Fig. 6. Taken together, the current results illustrate the possibility of controlling the formation of Ca-deficient apatite within near physiologic pH conditions that were maintained by the controlled swelling and degradation of PN-EA nanofibers.

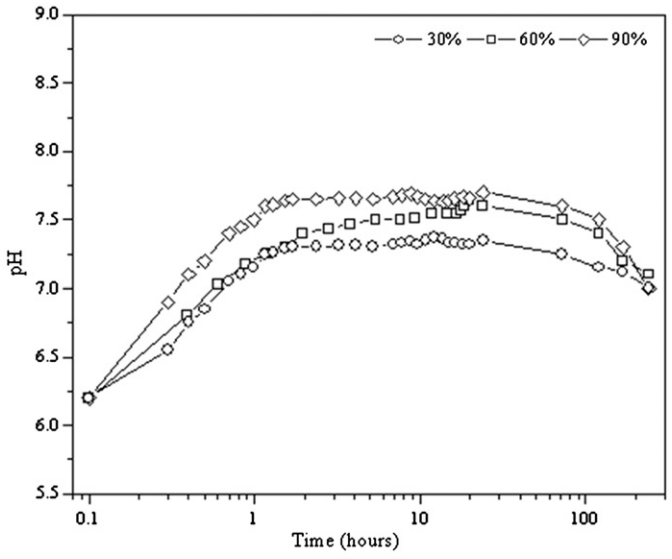

Fig. 9. Variation of pH of a solution containing PN-EA nanofibrous scaffolds containing 30, 60, and 90 wt % CDSH during hydrolysis in aqueous media for 10 days.

4. Summary

Nanofibrous composite scaffolds made of a biodegradable alanine-substituted polyphosphazene loaded with different proportions of Ca-deficient apatite precursors were prepared using an electrospinning technique. Precursors were evenly and homogenously distributed within the nanofibrous polymeric scaffold. Inclusion of the precursors within the scaffolds nanofibers resulted in a decrease of the surface area of the fibers. Hydrolysis of the composite scaffolds for up to 10 days in a PBS buffer solution resulted in a delayed conversion of the precursors into CDSH accompanied by swelling and degradation of the nanofibers. This in turn was also reflected in a pronounced decrease in the porosity of the composite scaffolds. Due to the encapsulation of the precursors within the nanofibers and the buffering effect resulting from the degradation of the polymer nanofibers, the process of formation of CDSH was maintained at near-physiologic pH conditions. Results shown in the current study illustrate the possibility of controlling the pH of hydrolysis of CDSH precursors by inclusion within biodegradable polymeric nanofibers, which undergo swelling and degradation to maintain pH conditions within physiologic values. It is strongly thought that these composite scaffolds will provide a template for bone regeneration. This is attributed to the fact that the pH-modulated dissolution–re-precipitation of the calcium-deficient apatitic precursors used in the current study will take part in the natural bone re-modeling process after implantation. The studied composite scaffolds are therefore recommended for further investigations to confirm their potential application in bone tissue regeneration.

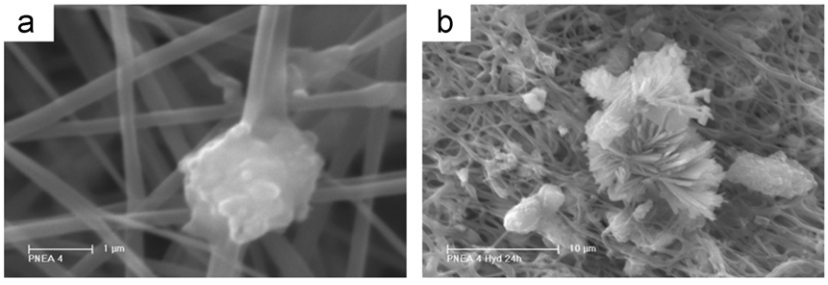

Fig. 10. Scanning electron micrographs of PN-EA nanofibrous scaffolds containing 90 wt% of CDSH precursors (a) as spun and (b) after hydrolysis for 10 days in aqueous media showing growth of Ca-deficient apatite crystals.

References

[1] M.M. Stevens, J.H. George, Exploring and engineering the cell surface interface, Science 310 (2005) 1135.

[2] W.E. Brown, L.C.A. Chow, New calcium phosphate water-setting cement, in: P.W. Brown (Ed.), Cements Research Progress, American Ceramic Society, Westerville, OH, 1987.

[3] Y.E. Greish, P.W. Brown, Phase evolution during the formation of stoichiometric hydroxyapatite at 37.4 °C, Journal of Biomedical Materials Research Part B: Applied Biomaterials 67B (2003) 632.

[4] M.T. Fulmer, R.I. Martin, P.W. Brown, Formation of calcium deficient hydroxyapatite at near-physiological temperature, Journal of Materials Science: Materials in Medicine 3 (1992) 299.

[5] R.I. Martin, K.S. TenHuisen, P. Leamy, P.W. Brown, Enthalpies of formation of compounds in the P_2O_5–CaO–H_2O system, Journal of Physical Chemistry B 101 (1997) 9375.

[6] H. Monma, T. Kanazawa, Hydration of α-tricalcium phosphate, Journal of Ceramic Society of Japan 108 (2000) S75.

[7] K.S. TenHuisen, P.W. Brown, The kinetics of calcium deficient and stoichiometric hydroxyapatite formation from $CaHPO_4 \cdot 2H_2O$ and $Ca_4(PO_4)_2O$, Journal of Materials Science: Materials in Medicine 7 (1996) 309.

[8] M.P. Ginebra, E. Fernandez, E.A.P. De Maeyer, R.M.H. Verbeeck, M.G. Boltong, J. Ginegra, Setting reaction and hardening of an apatite calcium phosphate cement, Journal of Dental Research 76 (1997) 905.

[9] R. Holmes, V. Mooney, R. Bucholz, A. Tencer, A coralline hydroxyapatite bone graft substitute, Clinical Orthopaedics and Related Research 188 (1984) 252.

[10] S. Sethuraman, L.S. Nair, S. El-Amin, M.N. Nguyen, Y.E. Greish, J.D. Bender, P.W. Brown, H.R. Allcock, C.T. Laurencin1, Novel low temperature setting nanocrystalline calcium phosphate cements for bone repair: osteoblast cellular response and gene expression studies, Journal of Biomedical Materials Research 82A (2007) 884.

[11] P.W. Brown, Calcium phosphates in biomedical engineering, in: K.H.J. Buschow et al.(Ed.), Encyclopedia of Materials Science and Technology, Elsevier, Oxford, 2001.

[12] R.I. Martin, P.W. Brown, Aqueous formation of hydroxyapatite, Journal of Biomedical Materials Research 35 (1997) 299.

[13] C. Durucan, P.W. Brown, Kinetic model for α-tricalcium phosphate hydrolysis, Journal of the American Ceramic Society 85 (2002) 2013.

[14] L.A. Dos Santos, L.C. De Oliveira, E.C.S. Rigo, R.G. Carrodeguas, A.O. Boschi, A.C.F. De Arruda, Influence of polymeric additives on the mechanical properties of α-tricalcium phosphate cement, Bone 25 (1999) 99S.

[15] C. Durucan, P.W. Brown, Low temperature formation of calcium-deficient hydroxyapatite-PLA/PLGA composites, Journal of Biomedical Materials Research 51 (2000) 717.

[16] X.Z. Zhou, V.Y. Leung, Q.R. Dong, K.M. Cheung, D. Chan, W.W. Lu, Mesenchymal stem cell-based repair of articular cartilage with polyglycolic acid–hydroxyapatite biphasic scaffold, International Journal of Artificial Organs 31 (2008) 480.

[17] C. Durucan, P.W. Brown, Calcium-deficient hydroxyapatite-PLGA composites: mechanical and microstructural investigation, Journal of Biomedical Materials Research 51 (2000) 726.

[18] F.E. Wiria, K.F. Leong, C.K. Chua, Y. Liu, Poly-ε-caprolactone/hydroxyapatite for tissue engineering scaffold fabrication via selective laser sintering, Acta Biomaterialia 3 (2007) 1.

[19] A.M. Ambrosio, H.R. Allcock, D.S. Katti, C.T. Laurencin, Degradable polyphosphazene/poly(α-hydroxy ester) blends: degradation studies, Biomaterials 23 (2002) 1667.

[20] O.M. Bostman, Osteoarthritis of the ankle after foreign-body reaction to absorbable pins and screws: a three to nine year follow-up study, Journal of Bone and Joint Surgery, British Volume 80 (1998) 333.

[21] L.S. Nair, D.S. Katti, C.T. Laurencin, Biodegradable polyphosphazenes for drug delivery applications, Advanced Drug Delivery Review 55 (2003) 467.

[22] H.R. Allcock, Chemistry and Applications of Polyphosphazenes, Wiley Interscience, New Jersey, 2004.

[23] N.N. Aldini, M.R. Fini, GG Giavaresi, Guided regeneration with resorbable conduits in experimental peripheral nerve injuries, International Orthopaedics 24 (2004) 121.

[24] S. Sethuraman, L.S. Nair, A. Singh, J.D. Bender, Y.E. Greish, P.W. Brown, H.R. Allcock, C.T. Laurencin, Development of novel biodegradable amino acid ester based polyphosphazenehydroxyapatite composites for bone tissue engineering, Materials Research Society Symposium Proceedings 845 (2005) 291.

[25] S. Bhattacharyya, L.S. Nair, J.D. Bender, Y.E. Greish, P.W. Brown, H.R. Allcock, C.T. Laurencin, Preparation of poly[bis(carboxylato phenoxy)phosphazene] non-woven nanofibers mats by electrospinning, Materials Research Society Symposium Proceedings (2004) 157 EXS-1.

[26] S. Sethuraman, L.S. Nair, M.T. Nguyen, A. Singh, N. Krogman, Y.E. Greish, P.W. Brown, H.R. Allcock, C.T. Laurencin, Design of high strength degradable polyphosphazenes: modulation of mechanical properties via side chain chemistry, Materials Research Society Symposium, Symposium Y: Mechanical Properties of Bio-inspired and Biological Materials (2004) (Fall 2004).

[27] S. Sethuraman, L.S. Nair, M.T. Nguyen, A. Singh, H.R. Allcock, Y.E. Greish, P.W. Brown, C.T. Laurencin, In vivo biocompatibility evaluation of novel amino acid ester based biodegradable polyphosphazenes for biomedical applications. In: Proceedings of the Transactions of the 30th Annual Meeting of the Society for Biomaterials, Nanotechnology and Biomaterials Symposium IV—Tissue and Cellular Engineering, vol. 187, 2005.

[28] S. Bhattacharyya, S.G. Kumbar, Y.M. Khan, L.S. Nair, A. Singh, N.R. Krogman, P.W. Brown, H.R. Allcock, C.T. Laurencin, Biodegradable polyphosphazene–nanohydroxyapatite composite nanofibers: scaffolds for bone tissue engineering, Journal of Biomedical Nanotechnology 5 (2009) 69.

[29] Y.E. Greish, J.L. Sturgeon, A. Singh, N.R. Krogman, A.H. Touny, S. Sethuraman, L.S. Nair, C.T. Laurencin, H.R. Allcock, P.W. Brown, Formation and properties of composites comprised of calcium-deficient hydroxyapatites and ethyl alanate polyphosphazenes, Journal of Materials Science: Materials in Medicine 19 (2008) 3153.

[30] Y.E. Greish, P.W. Brown, Hydrolysis of tetracalcium phosphate in the presence of a poly(alkenoic acid), Journal of Materials Research 14 (1999) 4637.

[31] S. Bhattacharyya, L.S. Nair, A. Singh, N.R. Krogman, Y.E. Greish, P.W. Brown, H.R. Allcock, C.T. Laurencin, Electrospinning of poly-[bis(ethyl alanato) phosphazene] nanofibers, Journal of Biomedical Nanotechnology 2 (2006) 36.

[32] A. Singh, N.R. Krogman, S. Sethuraman, L.S. Nair, J.L. Sturgeon, P.W. Brown, C.T. Laurencin, H.R. Allcock, Effect of side group chemistry on the properties of biodegradable L-alanine cosubstituted polyphosphazenes, Biomacromolecules 7 (2006) 914.